

A Combination of Docking/Dynamics Simulations and Pharmacophoric Modeling To Discover New Dual c-Src/Abl Kinase Inhibitors

Fabrizio Manetti,[†] Giada A. Locatelli,[‡] Giovanni Maga,[‡] Silvia Schenone,[§] Michele Modugno,[†] Stefano Forli,[†] Federico Corelli,[†] and Maurizio Botta^{*,†}

Dipartimento Farmaco Chimico Tecnologico, Università degli Studi di Siena, Via Alcide de Gasperi 2, I-53100, Siena, Italy, Istituto di Genetica Molecolare, IGM-CNR, Via Abbiategrasso 207, I-27100, Pavia, Italy, and Dipartimento di Scienze Farmaceutiche, Università degli Studi di Genova, Viale Benedetto XV 3, I-16132, Genova, Italy

Received March 1, 2006

A computational protocol was applied to identify molecular scaffolds untested toward the c-Src tyrosine kinase. A combination of docking and dynamics calculations allowed us to build three-dimensional models of the complexes between Src and several of its known inhibitors. Interactions most contributing to activity of the inhibitors, in terms of hydrogen bonds and hydrophobic contacts, were codified into pharmacophoric models that were in turn applied to perform a search of commercially available compounds within the Asinex database. As a result, we identified 1,3,4-thiadiazoles and pyrazolydine-3,5-diones showing inhibitory activity in the submicromolar range in a cell-free assay toward Src. Moreover, since several of the compounds used to generate pharmacophores were also known as Abl inhibitors, we tested the identified hits toward Abl tyrosine kinase, finding activity in the submicromolar range. Such biological data suggested that the computational protocol is an efficient tool for identifying new hits toward both Src and Abl.

Introduction

In the past 20 years, there has been a plethora of studies demonstrating that c-Src plays an important role in the signaling changes in the steps of cellular adhesion and motility,¹ as well as in the growth, progression, and metastasis of a variety of human malignancies. In fact, Src activation has been associated with colon, breast, pancreas, lung, and brain cancers.² Moreover, Src is also involved in biological pathways whose deregulation causes osteoporosis and metastatic bone diseases.³ These experimental findings are crucial keys to guide efforts aimed at identifying new low molecular weight compounds able to inhibit Src and, thus, to modulate aberrant pathways leading to malignant transformation of cells.

Members of the Src family kinases (SFKs) show a significant homology with Abl, whose kinase domain translocation on chromosome 9 induces proliferation of stem cells in the bone marrow and causes the chronic myelogenous leukemia (CML). The close homology between SFKs and Abl led to the experimental finding that structurally different compounds identified as Src inhibitors were later also described as Abl inhibitors. Such compounds [i.e., *N*5-(2-chloro-6-methylphenyl)-2-({6-[4-(2-hydroxyethyl)piperazin-1-yl]-2-methylpyrimidin-4-yl}amino)-1,3-thiazole-5-carboxamide (**1**), reported as BMS-354825⁴ and 6-(2,6-dichlorophenyl)-8-methyl-2-{{3-(methylthio)phenyl}amino}pyrido[2,3-*d*]pyrimidin-7(8*H*)-one (**2**), reported as PD173955, Chart 1]⁵ are now referred to as dual Src/Abl kinase inhibitors.

Although a huge number of compounds, potent and selective toward SFKs, are continuously designed and synthesized, there is no approved drug acting as Src inhibitor, yet. Many of these compounds are ATP-competitive inhibitors belonging to different chemical classes. As examples, quinoline derivatives

Chart 1. Structure of Template Inhibitors

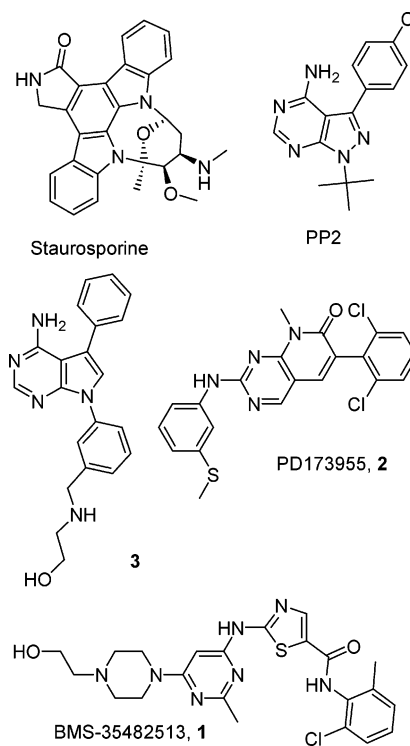


exhibit activity values up to the subnanomolar range in enzymatic assays and in the nanomolar range in Src-dependent cell proliferation assays.⁶ Additional classes of important Src inhibitors are quinazoline⁷ and pyrimidine derivatives. Among the latter, various pyrrolo-⁸ and pyrazolo-pyrimidines⁹ (such as 1-(*tert*-butyl)-3-(4-chlorophenyl)-4-amino-1*H*-pyrazolo[3,4-*d*]pyrimidine, PP2, Chart 1)¹⁰ were described.

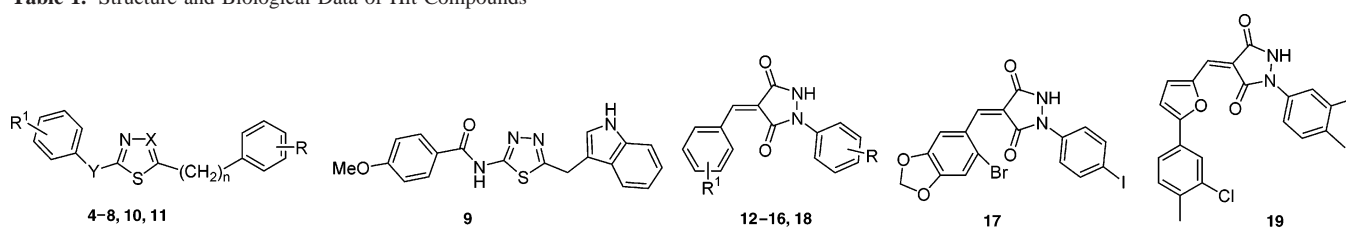
Herein, we report the application of a computational protocol based on molecular docking and dynamics simulations combined with a pharmacophore-based database search aimed at identifying hit compounds with molecular scaffold previously untested

* Maurizio Botta, Dipartimento Farmaco Chimico Tecnologico, Università degli Studi di Siena, Via Alcide de Gasperi 2, I-53100, Siena, Italy. Tel: +39 0577 234306, Fax: +39 0577 234333, email: botta@unisi.it.

[†] Università degli Studi di Siena.

[‡] Istituto di Genetica Molecolare.

[§] Università degli Studi di Genova.

Table 1. Structure and Biological Data of Hit Compounds


compd ^a	n	X	Y	R	R ¹	activity (K_i values, μM)	
						Src ^b	Abl ^c
BAS0338868, 4	2	N	CONH	H	H	2.9 ± 0.2	NA
BAS0338876, 5	2	N	CONH	H	4-I	NA	0.4 ± 0.1
BAS0338872, 6	2	N	CONH	H	2-I	2.0 ± 0.3	1.3 ± 0.3
BAS450225, 7	2	N	CONH	H	2,4-diCl	1.3 ± 0.4	NA
BAS09534324, 8	2	N	CONH	H	2-MeO, 4-MeS	4.1 ± 0.3	2.0 ± 0.2
BAS4844343, 9						1.9 ± 0.2	NA
BAS0321734, 10	1	N	NHCONH	H	H	NA	58 ± 5
BAS0140218, 11	0	CH	CONH	4-Me	4-Br	NA	NA
BAS01047655, 12				H	2-PhCH ₂ O	0.9 ± 0.1	NA
BAS00387347, 13				4-I	H	4.3 ± 0.4	0.6 ± 0.1
BAS00387328, 14				4-I	4-I	0.5 ± 0.1	0.8 ± 0.2
BAS01047341, 15				4-I	2-OH, 4-NEt ₂	1.0 ± 0.2	NA
BAS00387334, 16				4-I	4-(1-morpholino)	NA	20 ± 3
BAS00387275, 17						0.5 ± 0.1	2.5 ± 0.3
BAS00672722, 18				3,4-diCl	3-PhCH ₂ O	5.4 ± 0.4	1.0 ± 0.1
BAS01373578, 19						1.0 ± 0.1	5.0 ± 0.7
PP2						0.5 ± 0.1	0.5 ± 0.1

^a Compounds purchased from Asinex.²¹ ^b K_i values calculated from eq 2, where $E_0 = 0.0125 \mu\text{M}$ and $S_0 = 0.0160 \mu\text{M}$. NA = not active ($\text{ID}_{50} > 2 \text{ mM}$). ND = not determined. Values represent the mean of three independent experiments \pm SD. ^c K_i values calculated from eq 3, where $E_0 = 0.0125 \mu\text{M}$ and $S_0 = 0.0160 \mu\text{M}$. NA = not active ($\text{ID}_{50} > 2 \text{ mM}$). Values represent the mean of three independent experiments \pm SD.

as Src inhibitors. For this purpose, five known inhibitors of Src (hereafter referred to as the template inhibitors) with activity ranging from 300 to 0.5 nM and different molecular structure (Chart 1) were selected from the literature and docked into the ATP binding site of Src. The complexes obtained were submitted to molecular dynamics (MD) simulations for identifying the most significant interactions between Src and inhibitors, that were in turn encoded into pharmacophoric models. The latter were used as three-dimensional queries to screen a database of commercially available compounds for finding hits to be purchased and submitted directly to biological tests. All the tested compounds, with only one exception, were found to inhibit Src with an activity up to the submicromolar range. Moreover, since a couple of the template inhibitors used in our simulations (namely, **1** and **2**) are known as dual Src/Abl kinase inhibitors, we tested the identified hit compounds toward Abl, finding inhibitory activities up to the submicromolar range.

Biology. The mechanism of kinase inhibition was investigated using a cell-free assay with recombinant c-Src and Abl. Results showed that several of the compounds tested were characterized by an inhibitory activity toward the isolate Src in the micro- and submicromolar range (Table 1). The mechanism of inhibition was found to be competitive with the ATP substrate but not with a peptide used as a Src substrate.¹¹ On the other hand, similar studies on isolated Abl showed that the compounds were purely noncompetitive inhibitors with respect to both the ATP and the peptide substrates.

Results and Discussion

The crystallographic structure of the human c-Src (entry 2src of the Brookhaven protein data bank) was chosen as the starting point to perform molecular docking and MD simulations, although it represents Src in the catalytically inactive form (i.e., without phosphorylation at Tyr419, human numbering).¹² To support this choice, a comparison of the ATP binding site of

both Src and Lck (entry 1qpc of the Brookhaven protein data bank,¹³ whose structure with the catalytic domain in the active form is generally used for homology modeling of the structure of Src in its active form) was performed. The two structures were superposed on the basis of their backbone atoms within a 5 Å shell from the common cocrystallized inhibitor (phosphoaminophosphonic acid-adenylate ester, ANP). A root-mean-square deviation (rmsd) of 0.34 Å was found, suggesting a great similarity between ATP binding sites. Such pockets also showed a comparable volume and surface area (8448 Å³ and 2927 Å² for Src, 9053 Å³ and 2721 Å² for Lck), further supporting the hypothesis that both regions have a very similar topology, in terms of size and shape.

In the next step, a set of five known inhibitors of Src, belonging to different structural classes, were collected from the literature, with IC_{50} values ranging between 300 and 0.5 nM (Chart 1). The template inhibitors were docked into the optimized structure of Src by means of Autodock 3.0¹⁴ (suggested to be a reliable docking tool, see Supporting Information), and the resulting complexes were further minimized to overcome the major limitation of the software (namely, the protein rigidity). Inspection of docking results suggested two different binding modes (Figure 1). The first binding mode, according to a pharmacophoric model previously reported,¹⁵ showed the inhibitors [namely, staurosporine,¹⁶ PP2,¹⁰ and 2-{[3-(4-amino-5-phenyl-7H-pyrrolo[2,3-d]pyrimidin-7-yl)benzyl]amino}-ethanol,¹⁷ (**3**)¹⁸ involved in a hydrogen bonding network with the NH group of Met341 as a donor and the backbone carbonyl group of Glu339 as an acceptor, while an additional hydrogen bond occurred in the solvent accessible area (Asp404 with staurosporine and Lys295 with **3**). Moreover, a hydrophobic interaction was found between inhibitors and the hydrophobic region I, while their heteroaromatic scaffold was located within the adenine region. In the second binding mode, inhibitors such as **1** and **2** retained the interaction with the hydrophobic region

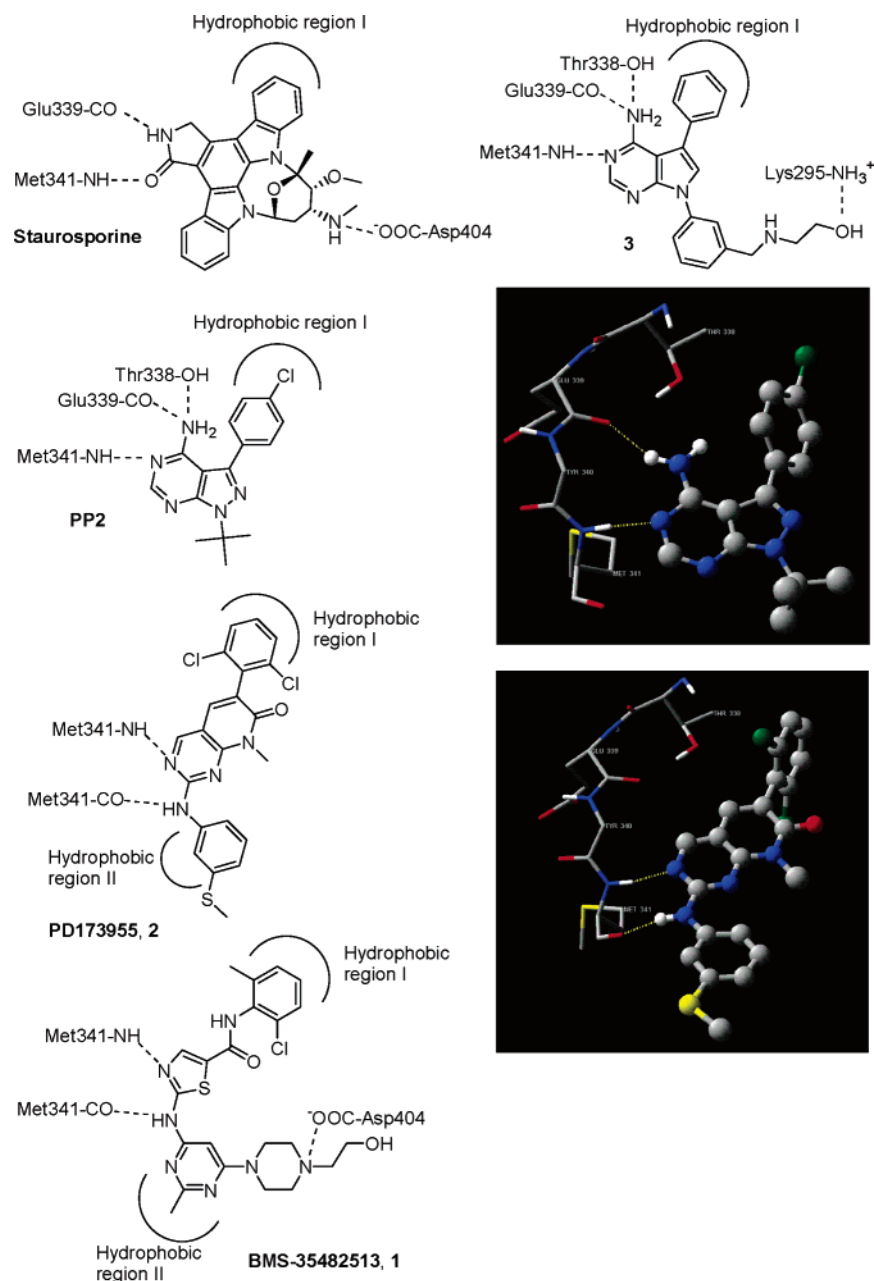


Figure 1. Schematic representation of the two different binding modes found for the template inhibitors by means of docking simulations followed by energy minimization of the obtained complexes. Staurosporine, **3**, and PP2 show a hydrogen bond donor–acceptor motif involving Glu339 and Met341, while PD173955 (**2**) and BMS-35482513 (**1**) interact with both the amide and carbonyl moieties of the Met341 backbone. For the sake of clarity, only hydrogen bond contacts and the major hydrophobic interactions are represented. As a representative example of both binding modes, a picture (black background) showing the major interactions (i.e., hydrogen bonds represented by yellow dotted lines) of PP2 (top) and **2** (bottom) with the Src binding site is also reported.

I. However, the hydrogen bond acceptor–donor motif¹⁹ was different with respect to that described in the first binding mode. In fact, NH and CO of Met341 backbone interacted with appropriate inhibitor counterparts to establish hydrogen bonds. As a consequence, the spatial location of the hydrogen bond donor group of the inhibitors was different from that found for inhibitors in the first binding mode. Compound **1** showed additional hydrogen bond contacts between its amido NH and the hydroxy of Thr338, and between the most basic nitrogen atom of the piperazine ring and the carboxy group of Asp404.

In summary, docking simulations showed two different binding modes for the template inhibitors. However, common interactions with the Src binding site were found. In fact, template inhibitors are characterized by a hydrogen bond contact with the backbone NH of Met341, a hydrophobic interaction

with the hydrophobic region I, and a common location of their scaffold within the adenine region. The hydrogen bond donor–acceptor motif (already proposed as a crucial key for kinase inhibitory activity) was completed by an interaction between a hydrogen bond donor on the inhibitor structure and a corresponding receptor counterpart represented by the carbonyl group of Met341 or, alternately, the terminal carboxylate of Glu339, allowing us to identify two binding modes. Additional interactions with Thr338, amino acids of the solvent accessible surface and the hydrophobic region II were also found with lower frequency.

MD simulations followed by energy minimizations were performed on each Src–inhibitor complex obtained by means of docking calculations, with the aim of identifying persistent interactions between inhibitors and their binding site, to be

Table 2. Volume and Surface Area of the ANP Binding Site on Src (2src) and Abl (1qpc)

pdb entry	surface (Å ²)	volume (Å ³)	Surf/Vol ratio
2src	2927	8448	0.346
1qpc	2721	9053	0.300

transformed into pharmacophoric features. For this purpose, we chose to analyze hydrogen bond distances and frequency during the simulation time. In principle, a significant increase of the hydrogen bond distance is supposed to describe a system where the ligand moves apart from the protein, while a relatively fixed distance can be interpreted as a close and profitable interaction between ligand and protein. On the other hand, hydrogen bond frequency describes the ratio between the number of samples (snapshots of Src–inhibitor complexes collected during MD simulations) with a hydrogen bond and the total number of samples studied.

As a result (Table 3), the hydrogen bond involving the backbone NH of Met341 (common to all the inhibitors) was persistent during the simulation time (frequency ranging from 82 to 99%), leading to define such an interaction as the major contact between protein and inhibitors. On the other hand, concerning the first binding mode, the carbonyl group of Glu339 was involved in a hydrogen bond with a high frequency in the complex with both staurosporine and **3**. In contrast, in the complex with PP2, the frequency of such a contact was quite low (24%), probably due to the fact that the hydroxy group of Thr338 was a competitor (as a hydrogen bond acceptor group) of the Glu339 carbonyl oxygen. This result suggested that both the Glu339 carbonyl oxygen and the Thr338 hydroxy oxygen could act as hydrogen bond acceptors, competing for hydrogen bond donor counterparts of the inhibitor structures. Analysis of hydrogen bond frequency in complexes with compounds following the second binding mode suggested that the carbonyl oxygen of Met341 could be an anchor point for Src inhibitors, such an interaction occurring with a frequency of 98 and 51% for **1** and **2**, respectively. In addition, both compounds were also characterized by profitable hydrophobic interactions between one of their aromatic moieties and the hydrophobic region II.

It is important to point out that analysis of the complexes between Src and inhibitors allowed us to find a correlation between hydrogen bond frequency/hydrophobic contacts and the activity values. In fact, in the complex with PP2, possessing the lowest activity value among compounds following the first binding mode, the hydrogen bond with Glu339 was not highly conserved, probably contributing to destabilize the complex itself. On the other hand, staurosporine and **3**, showing a very similar interaction pathway with the corresponding receptor, had comparable inhibitory activity toward Src (40 and 10 nM, respectively). Compounds following the second binding mode showed an additional hydrophobic interaction (with the hydrophobic region II) with respect to compounds following the first binding mode. This interaction, in addition to hydrogen bond frequencies of 93 and 98% toward Met341, led **1** to have the best inhibitory activity among all the compounds studied (0.5 nM). The activity of **1** was probably also influenced by the additional hydrogen bond contact with the carbonyl group of Glu339. In contrast, **2**, with a less frequent hydrogen bond involving the carbonyl group of Met341 (51%), showed an activity of 18 nM.

These results support the following qualitative considerations regarding interactions between the hinge region of Src and its ligands (further details on the interactions are reported in

Supporting Information): (i) The hydrogen bond donor–acceptor motif seems to be a structural requirement for activity of inhibitors. Simulations showed that a network of hydrogen bonds with Met341, Thr338, and Glu339 (reported to be critical amino acids for the binding of the inhibitors to the Src hinge region) constrained the inhibitors within the hinge region of Src, with their molecular scaffolds accommodated into the adenine pocket. While the interaction involving the NH group of Met341 was found with very high frequency (92–98%), interactions where residues are the hydrogen bond acceptor group (namely, the backbone carbonyl of Glu339 and Met341, and the hydroxy group of Thr338) showed a broader range of frequency (24–99%). This result was in part due to the fact that Thr338 and Glu339 are competitors in establishing hydrogen bonds with the corresponding inhibitor counterparts. (ii) The frequency of hydrogen bond contacts involving Met341, Thr338 and Glu339 seems to account for the different activity of inhibitors toward Src. (iii) For several inhibitors, profitable interactions with the hydrophobic region II and hydrogen bond contacts with residues of the solvent accessible surface are suggested to be important for activity. However, within the solvent accessible region, inhibitors contacted amino acids through transient hydrogen bonds involving different residues. This is probably due to the fact that amino acid side chains in the solvent accessible region are characterized by a conformational freedom higher than that of residues buried into the hinge region.

Pharmacophoric Model Calculations. Results from molecular docking and MD calculations, in terms of principal interaction points between inhibitors and the Src binding site, were encoded into pharmacophoric models. Five different pharmacophores were built by means of the software Catalyst²⁰ (Figure 2), describing the two binding modes of inhibitors into the Src binding site (involving the carbonyl group of Glu339 and the NH of Met341 or both the carbonyl and the NH groups of Met341, respectively). All the models had two common features, represented by the hydrogen bond acceptor group encoding the interaction with the Met341 NH and a hydrophobic sphere accounting for contacts with the hydrophobic region I of the binding site. Differences concern the hydrogen bond donor (HBD) feature and the shape of each model. In particular, three models (based on compounds following the first binding mode into Src) showed the HBD1 feature accounting for the interaction with the carbonyl group of Glu339. Each of them was implemented with a shape derived from staurosporine or **3** or PP2 in their conformation found after MD and minimization. The remaining two models (based on compounds following the second binding mode into Src) were characterized by HBD2 accounting for contacts with the carbonyl group of Met341 and a shape derived from **1** or **2**.

As described above, several inhibitors are characterized by interactions with amino acids constituting part of the solvent accessible region. However, it was impossible to identify for each inhibitor a molecular portion that interacts with the same pocket of the solvent accessible region. In fact, functional groups of staurosporine, **1**, and **3** interacting with solvent accessible amino acids are located at a mean distance of approximately 2.5 Å. As a consequence, these interactions were considered as specific contacts of each inhibitor with Src binding site, and they were not codified into pharmacophoric features.

A pharmacophoric-based database search was then performed on the Asinex Gold database²¹ by means of the five models, with the aim of (i) finding possible hit compounds (Src inhibitors) to be submitted directly to biological tests avoiding

Table 3. Summary of Hydrogen Bond Monitoring during MD Simulations^a

compound	groups	hydrogen bonds ^a			frequency (%)	hydrophobic contact ^b
		distance (Å)	X-H...Y angle (deg)	H...Y-Z angle (deg)		
staurosporine	lactam CO–Met341 NH	1.85 ± 0.15	151 ± 14	150 ± 14	98	HRI
	lactam NH–Glu339 CO	1.90 ± 0.17	145 ± 12	157 ± 11	97	
	amino NH–Asp348 CO	3.98 ± 1.82	110 ± 41	127 ± 23	34	
PP2	endocyclic N5–Met341 NH	2.06 ± 0.19	157 ± 13	137 ± 12	96	HRI
	amino group at C4–Glu339 CO ^c	2.02 ± 0.20	112 ± 12	143 ± 14	24	
3	endocyclic N3–Met341 NH	2.01 ± 0.14	160 ± 12	135 ± 12	99	HRI
	amino group at C4–Glu339 CO ^d	1.95 ± 0.16	148 ± 10	156 ± 11	99	
	hydroxy group–Lys295 NH ₂	>4				
PD173955, 2	endocyclic N3–Met341 NH	2.01 ± 0.16	154 ± 13	114 ± 12	92	HRI, HRII
	amino group at C2–Met341 CO	2.41 ± 0.47	129 ± 14	155 ± 13	51	
BMS-35482513, 1	endocyclic N3–Met341 NH	2.19 ± 0.20	154 ± 11	120 ± 9	93	HRI, HRII
	amino group at C2–Met341 CO	1.86 ± 0.15	150 ± 13	160 ± 11	98	
	amido NH–Thr338 OH	>4				
	amido CO–Lys295 NH ₂	>4				
	piperazine N–Asp404 COO ⁻	>4				
	amido NH–Glu339 CO	2.57 ± 0.39	161 ± 12	164 ± 10	47	

^a Groups of inhibitor and residues are reported, together with geometric properties of the hydrogen bond interaction (distance and angles) and its frequency. Distance (Å) and angles (X–H...Y and H...Y–Z in degrees) of hydrogen bond contacts were median values calculated on all the MD snapshot analyzed. Frequency is defined as the ratio between snapshots characterized by that contact and the total number of snapshots analyzed. ^b Hydrophobic contacts account for the interaction with the hydrophobic region I (HRI) and II (HRII). ^c The hydroxy group of Thr338 was transiently involved (<10%) in a hydrogen bond interaction with the amino group at C4 of PP2. ^d The amino group at C4 of 3 was transiently involved (<1%) in a hydrogen bond interaction with the hydroxy group of Thr338, in addition to the contact with the carbonyl group of Glu339.

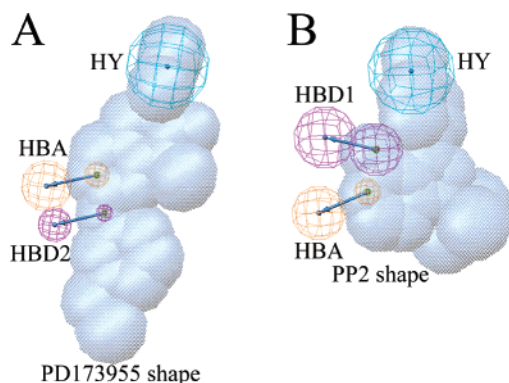


Figure 2. Examples of pharmacophoric models describing different binding modes of the template inhibitors into the hinge region of c-Src. Pharmacophoric features are color-coded: blue, hydrophobic (HY); orange, hydrogen bond acceptor (HBA); purple, hydrogen bond donors (HBD1 and HBD2). (A) Pharmacophoric model based on the orientation of PD173955 (**2**) into Src (referred to as the second binding mode in the text). HY is matched by the dichlorophenyl group at position 6 of the core able to interact with the hydrophobic region I of the receptor, HBA is the nitrogen atom at position 3 interacting with the NH moiety of Met341, HBD2 is the NH moiety at C2 interacting with the carbonyl group of Met341. The shape was calculated on the best conformer of **2** as obtained by docking and energy minimization of the corresponding complex. (B) Pharmacophoric model based on the orientation of PP2 into Src (referred to as the first binding mode in the text). HY is matched by the chlorophenyl group at position 3 of the core able to interact with the hydrophobic region I of the receptor, HBA is the nitrogen atom at position 5 interacting with the NH moiety of Met341, HBD1 is the NH₂ moiety at C4 interacting with the backbone carbonyl group of Glu339. The shape was calculated on the best conformer of PP2 as obtained by docking and energy minimization of the corresponding complex.

the resource-consuming step of synthesis and (ii) validating the pharmacophores themselves. A total number of about 250 000 known compounds were first pruned according to either their flexibility in terms of rotatable bonds or molecular weight. Next, they were submitted to an in silico screening by using the five pharmacophores as three-dimensional queries. Results from separate searches were ranked according to decreasing fit and shape similarity values. Inspection of the hit lists showed that the best ranked compounds belong to chemical classes charac-

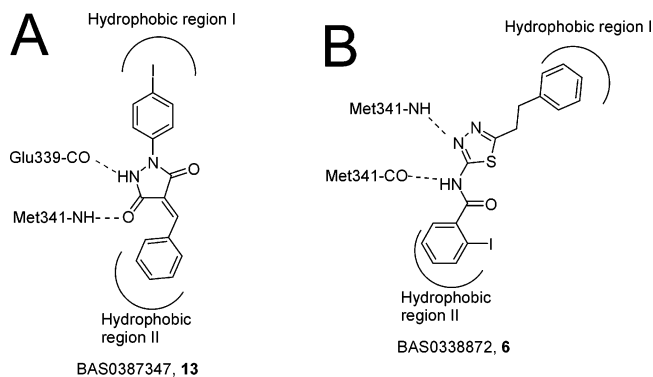


Figure 3. Schematic representation of the binding mode (in terms of hydrogen bonds and most profitable hydrophobic contacts) of two hit compounds into the hinge region of c-Src. (A) Compound **13** interacted with the receptor following the first binding mode, also found for PP2 and **3**. (B) Compound **6** showed contacts with amino acid residue involved in the second binding mode, similarly to that found for **1** and **2**.

terized by molecular scaffolds (namely, 1,3-thiazoles, 1,3,4-thiadiazoles, and pyrazolydine-3,5-diones) never tested toward Src. In a first step, only five compounds were selected and submitted to biological evaluation. Two of them showed an inhibitory activity toward the isolated Src enzyme in the micromolar range, while the remaining three compounds were inactive at the test dose. It is important to note that the active compounds [BAS0338872 (**6**), a thiadiazole derivative, and BAS0387347 (**13**), a pyrazolydine-3,5-dione, Table 1) were identified by using the pharmacophoric models based on the structure of **2** (Figure 2, A) and PP2 (Figure 2, B), respectively. Docking calculations on **6** showed that the major interactions involved N3 of the thiadiazole ring and the benzamide NH group that contacted by hydrogen bonds the NH and the carbonyl moieties of Met341, respectively (Figure 3, B), following the second binding mode (similarly to **1** and **2**). Moreover, hydrophobic profitable interactions were found between the phenylethyl side chain and the hydrophobic region I, and between the phenyl ring of the benzamido moiety and the hydrophobic region II. On the other hand, NH and the carbonyl of the lactam moiety of **13** interacted with the carbonyl group

of Glu339 and with the NH moiety of Met341, respectively (Figure 3, A), in a way similar to that found for PP2 and **3** (first binding mode). The iodophenyl chain contacted the hydrophobic region I, while the remaining phenyl group is partially embedded within the hydrophobic region II.

On the basis of biological results on **6** and **13** (Table 1), the ranking lists obtained with the above-mentioned models based on PP2 and **2** were further analyzed to find the next congeneric compounds belonging to the thiazazole and pyrazolydine-3,5-dione classes. A small set of additional 11 compounds were selected (four thiazazoles and seven pyrazolydine-3,5-diones) and submitted to biological tests. All of them showed an inhibitory activity ranging from 0.5 (comparable to that of PP2 used as the reference compound) to 5.4 μM (Table 1), with the sole exception of BAS00387334 (**16**) that was found inactive at the test dose.

Among phenylethyl thiazazoles, biological data showed that variously substituted benzamido moieties led to comparable activity toward Src. The only exception to this trend was BAS0338876 (**5**), bearing a *p*-I substituent, found to be inactive. Rigidification of the phenylethyl chain to an indolylmethyl moiety led to BAS4844343 (**9**) that retained a micromolar activity, while lengthening the benzamido chain to a phenylurea and shortening the phenylethyl to a benzyl chain gave the inactive compound BAS0321734 (**10**).

Regarding, N1-(4-Iodophenyl)pyrazolydine-3,5-diones, **13**, bearing an unsubstituted phenyl ring at position 4, showed an activity about 1 order of magnitude lower than the corresponding *p*-I derivative BAS00387328 (**14**) (4.3 versus 0.5 μM , respectively), suggesting that a substitution on this phenyl ring is profitable for activity. Compounds BAS00387275 (**17**) and BAS01047341 (**15**) had an activity value comparable (0.47 μM) or slightly lower (1 μM) with respect to **14**, respectively. Compound **16** was an exception, showing no appreciable activity toward Src at the test dose.

On the basis of the experimental evidence that various Src inhibitors were also found to be Abl inhibitors, compounds identified in the database search were also tested for their inhibitory activity toward Abl. As a result (Table 1), a comparison of activity toward Src and Abl showed that most compounds exerted a comparable inhibition. On the contrary, while five compounds showed appreciable Src selectivity [namely, BAS0033868 (**4**), BAS00450225 (**7**), **9**, BAS01047655 (**12**), and **15**, with an activity ratio >70], **5** was the sole compound to have a submicromolar activity toward Abl (0.4 μM), with no inhibition of Src (activity ratio >500).

In conclusion, we report in the paper the application of an efficient computational protocol based on docking/MD simulations and a pharmacophore-based database search that led to the identification of commercially available compounds showing significant inhibitory activity toward both Src and Abl, comparable to that found for PP2 used as the reference compound. Although the new compounds cannot be considered as potential clinical candidates, their molecular scaffold (original in the field of both Src and Abl inhibitors) combined with their biological properties (good activity and/or selectivity) allowed us to classify such compounds as promising hits in the search for new tyrosine kinase inhibitors.

Experimental Section

Biology. Enzymatic Assay on Isolated Src. Recombinant human Src was purchased from Upstate (Lake Placid, NY). Activity was measured in a filter-binding assay using a commercial kit (Src Assay Kit, Upstate), according to the manufacturer's protocol, using 150 μM of the specific Src peptide substrate (KVEKIGEGTYGVVYK)

and in the presence of 0.125 pmol of Src and 0.160 pmol of [γ -³²P]-ATP. The apparent affinity (K_m) values of the Src preparation used for its peptide and ATP substrates were determined separately and found to be 30 μM and 5 μM , respectively.

Kinetic Analysis. Dose-response curves were generated by fitting the data by computer simulation to eq 1: $E_{(\%)}$ = $E_{\text{max}}/(1 + [I]/ID_{50})$, where $E_{(\%)}$ is the fraction of the enzyme activity measured in the presence of the inhibitor, E_{max} is the activity in the absence of the inhibitor, $[I]$ is the inhibitor concentration, and ID_{50} is the inhibitor concentration at which $E_{(\%)} = 0.5E_{\text{max}}$.

The ID_{50} were converted to K_i according to a competitive mechanism with respect to the substrate ATP. The second substrate of the reaction (the peptide) was kept at saturating concentrations (4-fold higher its K_m). Since (i) the ATP concentration was limiting, i.e., $[ATP] \ll K_{m(ATP)}$, and (ii) the enzyme concentration was not negligible with respect to the ATP concentration, i.e., $[E] \geq [ATP]$, the classical Cheng-Prusoff relationship was not applicable. Consequently, K_i values were calculated according to eq 2: $K_i = (ID_{50} - E_0/2)/\{E_0 - [S_0/K_m - 1]/E_0\}$, where S_0 is the concentration of the competing substrate (ATP) and E_0 is the concentration of the enzyme. Each experiment was done in triplicate and mean values were used for the interpolation. Curve fitting was performed with the program GraphPad Prism.

Enzymatic Assay on Isolated Abl. Recombinant human Abl was purchased from Upstate. Activity was measured in a filter-binding assay using an Abl specific peptide substrate (Abtide, Upstate). Reaction conditions were: 0.012 μM [γ -³²P]ATP, 50 μM peptide, 0.022 μM *c*-Abl. The apparent affinity (K_m) values of the Abl preparation used for its peptide and ATP substrates were determined separately and found to be 1.5 μM and 10 μM , respectively. Kinetic analysis was performed as described for *c*-Src. Due to the noncompetitive mode of action and to the fact that the enzyme concentration was higher than the ATP substrate concentration, ID_{50} values were converted to K_i by eq 3: $K_i = ID_{50}\{E_0 + [E_0(K_{m(ATP)}/S_0)]\}/E_0$, where E_0 and S_0 are the enzyme and the ATP concentrations, respectively. Each experiment was done in triplicate and mean values were used for the interpolation. Curve fitting was performed with the program GraphPad Prism.

Computational Details. All calculations and graphic manipulations were performed on Intel Xeon 3 GHz and SGI 12K processors.

Superposition of Macromolecular Structures. Crystallographic structures of 2src and 1qpc were aligned on the basis of their common inhibitor ANP and each amino acid having at least one atom within a 5 Å distance from ANP. Only coordinates of amino acid backbone atoms and inhibitor heavy atoms were considered during superposition, finding a rmsd of 0.34 Å.

Calculations of Volume and Surface of the Hinge Region (*c*-Src and Lck). The program Grid 2.2²² was used to define a grid (point space of 0.5 Å) around the hinge region of both structures and to calculate interaction maps for the probe water. Grid maps for water were imported into VolSurf 4.0²³ to calculate both molecular surface and volume of the hinge region of Src and Lck. In particular, VolSurf molecular surface represents the accessible surface (in Å²) traced out by a water probe interacting at 0.20 kcal/mol when rolling over the target molecule, while molecular volume represents the water solvent excluded volume (in Å³), i.e., the volume contained within the water accessible surface computed at 0.20 kcal/mol. The volume of the hinge cavities was then calculated by the difference between the volume of the grid extended to the whole hinge region (including amino acids) and the molecular volume as obtained by VolSurf: $\text{Vol}_{\text{cavity}} = \text{Vol}_{\text{grid}} - \text{Vol}_{\text{mol}}$. Data summarized in Table 2, reporting size and extension of the hinge regions, showed that only a 6.7% difference was observed among volumes, supporting the hypothesis that hinge regions of Src and Lck are very similar in size and shape (since they accommodated the same inhibitor).

Docking Calculations. Structures of template inhibitors were represented using MacroModel²⁴ and minimized with the Amber* force field using the Polak-Ribiere conjugated gradient method (0.001 kJ/mol·Å convergence or 10 000 iterations). Mopac was applied to calculate ESP charges with the MNDO approximation.

To be exported to Autodock, the minimized structures were converted into the mol2 file format using Babel software. The reliability of the docking protocol was first tested by simulations of the binding mode of tyrosine kinase inhibitors (Gleevec, 2, staurosporine, and PP2) and comparison of the modeled complexes with the available three-dimensional structures derived by X-ray crystallography (1opj,²⁵ 1m52,^{5b} 1qpd,¹³ and 1qpe).¹³ The program successfully reproduced the X-ray coordinates of the inhibitor binding conformations (rmsd values ranging from 0.4 to 1.0 Å between docked and crystallographic conformers), as well as the features of pharmacophoric models reported in the literature.¹⁵ The ability to accurately predict the binding conformation of various inhibitors suggested that Autodock would exhibit a similar accuracy with the same compounds when docked into the c-Src binding site.

Having a reliable docking procedure in our hands, in the next step of the computational work, we used the crystallographic structure of Src (2src) to dock template compounds. To remove unfavorable contacts, a preliminary structure optimization was performed through the all-atom Amber* force field and Polak-Ribiere conjugate gradient method. A continuum solvation method (GB/SA), with water as the solvent, was also applied. Extended cutoffs were used and convergence was set to 0.01 kJ/mol·Å. A rmsd value of 1.6 Å, calculated on the whole structure, was found, with no significant conformational rearrangement of the hinge region. The optimized Src structure was then used to perform docking calculations with template compounds, followed by a second minimization (following the same protocol) mainly aimed at overcoming the major limitation of the docking software (i.e., receptor kept fixed). In detail, after minimization, Src was imported in Autodock Tools (ADT) and prepared for Autodock calculations by removing nonpolar hydrogens, while Kollman united-atom partial charges and solvent parameters were added. Similarly to the protein, the structure of the inhibitors was also prepared by deleting their nonpolar hydrogen atoms. Finally, the rigid root and rotatable bonds were defined using ADT.

During the next step, several atom probes (characterized by the same stereoelectronic properties as the atoms constituting the inhibitor) were moved on the grid nodes, while the interaction energy between the probe and the inhibitor was calculated at each node. In such a way, grid maps can be generated for each atom probe, describing its interactions with the inhibitor. Autogrid 3.0, as implemented in the Autodock 3.0 software package, was used to generate grid maps.

The Lamarckian genetic algorithm (LGA)¹⁴ was employed to generate orientations/conformations of the ligand within the binding site. Parameters for docking runs were set as follows (imported from a docking parameter file), on the basis of literature suggestions.²⁶ The choice of the best conformation was based on the

outlev 1	diagnostic output level
rmstol 1.5	cluster_tolerance/A
extnrg 1000.0	external grid energy
e0max 0.0 10000	max initial energy; max number of retries
ga_pop_size 500	number of individuals in population
ga_num_evals 10000000	maximum number of energy evaluations
ga_num_generations 1000000	maximum number of generations
ga_elitism 1	number of top individuals to survive to next generation
ga_mutation_rate 0.02	rate of gene mutation
ga_crossover_rate 0.8	rate of crossover
ga_window_size 10	
ga_cauchy_alpha 0.0	Alpha parameter of Cauchy distribution
ga_cauchy_beta 1.0	Beta parameter Cauchy distribution
set_ga	set the above parameters for GA or LGA
sw_max_its 300	iterations of Solis & Wets local search
sw_max_succ 4	consecutive successes before changing rho
sw_max_fail 4	consecutive failures before changing rho
sw_rho 1.0	size of local search space to sample
sw_lb_rho 0.01	lower bound on rho
ls_search_freq 0.06	probability of performing local search on individual
set_psw1	set the above pseudo-Solis & Wets parameters
ga_run 250	do this many hybrid GA-LS runs
analysis	perform a ranked cluster analysis

assumption that, although for high throughput screening protocols, only the first ranked conformation should be considered (that is, the conformation characterized by the lowest estimated free energy of binding),²⁷ in other cases, the lowest energy conformation of the most populated cluster should also be taken into account.²⁸

Complexes derived from docking calculations were further submitted to an energy minimization protocol (same settings as above) to overcome the major limitation of the docking procedure (i.e., the structure of the receptor is kept fixed during all the calculations). However, because of the large number of atoms in the models, the following additional constraints had to be imposed: i. a subset, comprising only the inhibitor and a shell of residues possessing at least one atom at a distance of 6 Å from any of the inhibitor atoms, was created and subjected to energy minimization. The inhibitor and all the amino acid side chains of the shell were unconstrained during energy minimization to allow for reorientation and proper hydrogen bonding geometries and van der Waals contacts; ii. all the atoms not included in the above-defined subset were fixed, but their nonbond interactions with all the relaxing atoms were calculated. Further details on this computational protocol were reported elsewhere.²⁹

MD Calculations. Complexes derived from docking simulations and energy minimization were submitted to a MD protocol. MacroModel and the united-atom Amber* force field were used for MD simulations. GB/SA with water parameters was used to simulate the solvent. The starting structures were relaxed by performing 50 ps of MD at 310 K (equilibration phase). Next, each system was submitted to 1 ns of MD simulations (310 K), and snapshot structures were extracted for every 1 ps. A 25 kcal/mol constraint was imposed to pairs of atoms involved in hydrogen bond contacts stabilizing α helices and β sheets, when their distance raised to more than 5 Å during simulations. Moreover, amino acid atoms external to a 20 Å shell from the inhibitor atoms were kept fixed during MD.

Hydrogen bonds (identified in the complexed obtained from docking/minimization) involving inhibitors were monitored to check their length and frequency during the time of MD simulations. Three requisites are required for a contact to be considered as a hydrogen bond: (1) H...Y distance up to 2.5 Å, (2) X-H...Y angle $\geq 120^\circ$, (3) H...Y-Z angle $\geq 90^\circ$, where H is the hydrogen atom, X is the donor atom, Y is the acceptor atom, and Z is an atom covalently bound to Y.

Pharmacophoric Modeling. Pharmacophoric features used to generate models were defined as follows. The inclusion of a hydrogen bond acceptor (HBA) feature in a pharmacophoric model is aimed at accounting for the hydrogen bond contact between various acceptor atoms/groups on the inhibitor structures and the Met341 NH. Tolerance and weight of HBA were set to 0.75 Å and 3, respectively. In particular, the tolerance of the acceptor sphere was set to 0.75 Å because the acceptor atom of the template inhibitors are located in almost the same region of space. In fact, in the conformation of each inhibitor chosen for pharmacophoric modeling, the HBA atom was at a mean distance of 0.5 Å from the acceptor atoms of the remaining inhibitors. Moreover, MD showed that the distance between the acceptor atom on the inhibitors and the hydrogen atom of Met 341 NH was conserved (1.85–2.19 Å), with a very low standard deviation (<0.2 Å). Considering the fact that the HBA feature is representative of the contact involving the Met341 NH with inhibitors (the most frequent interaction found for all the inhibitors), we set a feature weight of 3 for it.

One of the two hydrogen bond donor features (namely, HBD1) is intended to codify for the interaction with the carbonyl group of Glu339 (in the first binding mode found during docking calculations) or the hydroxy group of Thr338, found to be competitors each other for a hydrogen bond contact with the donor group of PP2. On the basis of the fact that both the above-mentioned residues are able to perform such an interaction, the tolerance of the projection sphere of the feature (corresponding to the sphere accommodating the heteroatom bound to the hydrogen) was set to

2.00 Å. In a similar way, due to the different spatial position of the donor heavy atom of inhibitors, also the tolerance of the anchor sphere was set at the same value. Moreover, since this feature was very frequently found in staurosporine and **3**, but not in PP2, its weight was set to a value of 2, lower with respect to that of HBA found in all the complexes with almost quantitative frequency. The second hydrogen bond feature (HBD2) accounts for the interactions (found in the second binding mode during docking calculations) between a hydrogen bond donor group of both **1** and **2** with an acceptor on the receptor counterpart (the carboxyl of Met341). Considering the short interatomic distance (<0.5 Å) between the two donor heavy atoms of **1** and **2**, the tolerance was reduced to 0.5 Å, while the feature weight was set to 2.

Finally, the hydrophobic feature describes molecular portions able to interact with the hydrophobic region I. Since portions of the inhibitors lying within this pocket were not completely aligned each other and they, as a whole, did not completely fill the hydrophobic cavity of the receptor, the tolerance of such a feature was set to 2.5 Å. Moreover, since that all the inhibitors showed a profitable interaction with the hydrophobic region I, the weight of the feature was set to 3.

To perform a preliminary test on the reliability of the five pharmacophoric hypotheses, they were used as three-dimensional queries to search a small database of known tyrosine kinase inhibitors (a demo version of the Jubilant database, provided by Accelrys).³⁰ As a result, 95 putative c-Src inhibitors were identified by the models, among which 25 are known (real) inhibitors. Since the database contains 102 Src inhibitors among a total of about 2000 compounds, the enrichment factor was about 5.2. It is important to note that most inhibitors in the database are classified on the basis of their activity toward only a particular tyrosine kinase. As a consequence, it is possible that compounds tested toward a kinase different from c-Src could actually also be active toward Src itself, having only a positive effect on the enrichment factor reported.

The pharmacophoric-based search on the Asinex Gold database (about 250 000 compounds) was constrained by cutoffs on both molecular weight (compounds with a molecular weight higher than 500 were rejected) and number of rotatable bonds (compounds with a number of rotatable bonds higher than that of the compound used to generate the pharmacophoric shape were discarded). The latter constraint was imposed on the basis of the fact that ligands with a high degree of conformational freedom are usually disfavored in their binding, due to an unprofitable entropic contribution. Moreover, most of the Src inhibitors able to bind the hinge region are characterized by low flexibility.

Lists obtained by means of database searches were ranked according to the fit values and shape similarity, describing how well each compound was able to match the features and the shape of the pharmacophoric models, respectively, and thus accounting for the complementarity between each ligand and the c-Src binding site. Analysis of hit lists showed that the 2- and the PP2-based pharmacophores identified compounds characterized by the best fit (higher than 7.5 with respect to the maximum value of 8) and shape similarity values (higher than 0.7 with respect to the maximum value of 1), with respect to the models bearing the shape of the remaining three template inhibitors (namely, **1**, staurosporine, and **3**). As a consequence, we chose to select the five best ranked compounds (three from the 2-based search and two from the PP2-based search) to be purchased and tested. On the basis of biological results, the two hit lists were further analyzed to identify additional compounds belonging to the same structural classes of **6** (from the 2-based search) and **13** (from the PP2-based search), both of them showing an inhibitory activity toward Src in the micromolar range. An additional 11 compounds were selected and tested.

Acknowledgment. Financial support provided by the Italian MIUR (Cofin 2004-prot. 2004059221_004) and by the Fondazione Monte dei Paschi di Siena is gratefully acknowledged. We would like to thank Asinex for a partial financial support to the

work. We are also indebted with Prof. G. Cruciani (University of Perugia, Italy) for kindly providing us with the program VolSurf and with Dr. G. Gaviraghi (Sienabiotech S.p.A.) for helpful discussion. The “Centro Universitario per l’Informatica e la Telematica” of the University of Siena is also acknowledged.

Supporting Information Available: Details of preliminary docking simulations and description of the binding mode of template compounds. This material is available free of charge via the Internet at <http://pubs.acs.org>.

References

- (1) (a) Martin, G. S. The hunting of the Src. *Nat. Rev. Mol. Cell Biol.* **2001**, *2*, 467–475. (b) Frame, M. C.; Fincham, V. J.; Carragher, N. O.; Wyke, J. A. v-Src’s hold over actin and cell adhesions. *Nat. Rev. Mol. Cell Biol.* **2002**, *3*, 233–245. (c) Bjorge, J. D.; Jakymiw, A.; Fujita, D. J. Selected glimpses into the activation and function of Src kinase. *Oncogene* **2000**, *19*, 5620–5635.
- (2) (a) Mazurenko, N. N.; Kogan, E. A.; Zborovskaya, I. B.; Kissel’ov, F. L. Expression of pp60c-src in human small cell and non-small cell lung carcinomas. *Eur. J. Cancer* **1992**, *28*, 372–377. (b) Irby, R. B.; Yeatman, T. J. Role of Src expression and activation in human cancer. *Oncogene* **2000**, *19*, 5636–5642. (c) Budde, R. J.; Ke, S.; Levin, V. A. Activity of pp60c-src in 60 different cell lines derived from human tumors. *Cancer Biochem. Biophys.* **1994**, *14*, 171–175. (d) Irby, R. B.; Mao, W.; Coppola, D.; Kang, J.; Loubeau, J. M.; Trudeau, W.; Karl, R.; Fujita, D. J.; Jove, R.; Yeatman, T. J. Activating SRC mutation in a subset of advanced human colon cancers. *Nat. Genet.* **1999**, *21*, 187–190. (e) Verbeek, B. S.; Vroom, T. M.; Adriaansen-Slot, S. S.; Ottenhoff-Kalff, A. E.; Geertzema, J. G.; Hennipman, A.; Rijksen, G. c-Src protein expression is increased in human breast cancer. An immunohistochemical and biochemical analysis. *J. Pathol.* **1996**, *180*, 383–388.
- (3) Susa, M.; Missbach, M.; Green, J. Src Inhibitors: Drugs for the Treatment of Osteoporosis, Cancer, or Both? *Trends Pharmacol. Sci.* **2000**, *21*, 489–495.
- (4) Lombardo, L. J.; Lee, F. Y.; Chen, P.; Norris, D.; Barrish, J. C.; Behnia, K.; Castaneda, S.; Cornelius, L. A. M.; Das, J.; Doweyko, A. M.; Fairchild, C.; Hunt, J. T.; Inigo, I.; Johnston, K.; Kamath, A.; Kan, D.; Klei, H.; Marathe, P.; Pang, S.; Peterson, R.; Pitt, S.; Schieven, G. L.; Schmidt, R. J.; Tokarski, J.; Wen, M.-L.; Witayak, J.; Borzilleri, R. M. Discovery of N-(2-Chloro-6-methyl-phenyl)-2-(6-(4-(2-hydroxyethyl)-piperazin-1-yl)-2-methylpyrimidin-4-ylamino)thiazole-5-carboxamide (BMS-354825), a Dual Src/Abl Kinase Inhibitor with Potent Antitumor Activity in Preclinical Assays. *J. Med. Chem.* **2004**, *47*, 6658–6661.
- (5) (a) Moasser, M. M.; Srethapakdi, M.; Sachar, K. S.; Kraker, A. J.; Rosen, N. Inhibition of Src Kinases by a Selective Tyrosine Kinase Inhibitor Causes Mitotic Arrest. *Cancer Res.* **1999**, *59*, 6145–6152. (b) Nagar, B.; Bornmann, W. G.; Pellicena, P.; Schindler, T.; Veach, D. R.; Miller, W. T.; Clarkson, B.; Kuriyan, J. Crystal structures of the kinase domain of c-Abl in complex with the small molecule inhibitors PD173955 and imatinib (STI-571). *Cancer Res.* **2002**, *62*, 4236–4243. (c) O’Hare, T.; Pollock, R. M.; Stoffregen, E. P.; Keats, J. A.; Abdullah, O. M.; Moseson, E. M.; Rivera, V. M.; Tang, H.; Metcalf, C. A., III; Bohacek, R. S.; Wang, Y.; Sundaramoorthi, R.; Shakespeare, W. C.; Dalgarno, D.; Clackson, T.; Sawyer, T. K.; Deininger, M. W.; Druker, B. J. Inhibition of wild-type and mutant Bcr-Abl by AP23464, a potent ATP-based oncogenic protein kinase inhibitor: implications for CML. *Blood* **2004**, *104*, 2532–2539.
- (6) Barrios Sosa, A. C.; Boschelli, D. H.; Wu, B.; Wang, Y.; Golas, J. M. Further studies on ethenyl and ethynyl-4-phenylamino-3-quinolinecarbonitriles: identification of a subnanomolar Src kinase inhibitor. *Bioorg. Med. Chem. Lett.* **2005**, *15*, 1743–1747.
- (7) Plé, P. A.; Green, T. P.; Hennequin, L. F.; Curwen, J.; Fennel, M.; Allen, J.; Lambert-van der Brempt, C.; Costello, G. Discovery of a new class of anilinoquinazoline inhibitors with high affinity and specificity for the tyrosine kinase domain of c-Src. *J. Med. Chem.* **2004**, *47*, 871–887.
- (8) Altmann, E.; Widler, L.; Missbach, M. N(7)-substituted-5-arylpyrrolo[2,3-d]pyrimidines represent a versatile class of potent inhibitors of the tyrosine kinase c-Src. *Mini Rev. Med. Chem.* **2002**, *2*, 201–208.
- (9) (a) Schenone, S.; Bruno, O.; Ranise, A.; Bondavalli, F.; Brullo, C.; Fossa, P.; Mosti, L.; Menozzi, G.; Carraro, F.; Naldini, A.; Bernini, C.; Manetti, F.; Botta, M. New Pyrazolo[3,4-d]pyrimidines Endowed with A431 Antiproliferative Activity and Inhibitory Properties of Src Phosphorylation. *Bioorg. Med. Chem. Lett.* **2004**, *14*, 2511–2517. (b) Carraro, F.; Pucci, A.; Naldini, A.; Schenone, S.; Bruno, O.;

- Ranise, A.; Bondavalli, F.; Brullo, C.; Fossa, P.; Menozzi, M.; Mosti, L.; Manetti, F.; Botta, M. Pyrazolo[3,4-*d*]pyrimidines Endowed with Antiproliferative Activity on Ductal Infiltrating Carcinoma Cells. *J. Med. Chem.* **2004**, *47*, 1595–1598.
- (10) Hanke, J. H.; Gardner, J. P.; Dow, R. L.; Changelian, P. S.; Brissette, W. H.; Weringer, E. J.; Pollok, B. A.; Connelly, P. A. Discovery of a novel, potent, and Src family selective tyrosine kinase inhibitor. Study of Lck- and FynT-dependent T cell activation. *J. Biol. Chem.* **1996**, *271*, 695–701.
- (11) Maga, G. manuscript in preparation.
- (12) Xu, W.; Doshi, A.; Lei, M.; Eck, M. J.; Harrison, S. C. Crystal structures of c-Src reveal features of its autoinhibitory mechanism. *Mol. Cell* **1999**, *3*, 629–638.
- (13) Zhu, X.; Kim, J. L.; Newcomb, J. R.; Rose, P. E.; Stover, D. R.; Toledo, L. M.; Zhao, H.; Morgenstern, K. A. Structural analysis of the lymphocyte-specific kinase Lck in complex with nonselective and Src family selective kinase inhibitors. *Structure Fold. Des.* **1999**, *7*, 651–661.
- (14) Morris, G. M.; Goodsell, D. S.; Halliday, R. S.; Huey, R.; Hart, W. E.; Belew, R. K.; Olson, A. J. Automated Docking Using a Lamarckian Genetic Algorithm and Empirical Binding Free Energy Function. *J. Comput. Chem.* **1998**, *19*, 1639–1662.
- (15) Traxler, P.; Bold, G.; Frei, J.; Lang, M.; Lydon, N.; Mett, H.; Buchdunger, E.; Meyer, T.; Mueller, M.; Furet, P. Use of a pharmacophore model for the design of EGF-R tyrosine kinase inhibitors: 4-(phenylamino)pyrazolo[3,4-*d*]pyrimidines. *J. Med. Chem.* **1997**, *40*, 3601–16.
- (16) Omura, S.; Iwai, Y.; Hirano, A.; Nakagawa, A.; Awaya, J.; Tsuchiya, H.; Takahashi Y.; Masuma, R. New alkaloid AM-2282 of *Streptomyces* origin – taxonomy, fermentation, isolation and preliminary characterisation. *J. Antibiot.* **1977**, *30*, 275–282.
- (17) Missbach, M.; Altmann, E.; Widler, L.; Susa, M.; Buchdunger, E.; Mett, H.; Meyer, T.; Green, J. Substituted 5,7-diphenyl-pyrrolo[2,3-*d*]pyrimidines: potent inhibitors of the tyrosine kinase c-Src. *Bioorg. Med. Chem. Lett.* **2000**, *10*, 945–949.
- (18) Compound CGP62464 reported in ref 17 differs from **3** for the lack of the side chain on the phenyl ring at N7 of the pyrrolo-pyrimidine scaffold.
- (19) In the text, we use the term “hydrogen bond acceptor–donor motif” to describe two groups of the inhibitor structure. One of them is the hydrogen bond acceptor moiety interacting with the NH group of Met341 (i.e., the endocyclic N5 of PP2. The second one is the hydrogen bond donor group interacting with the carbonyl of Glu339 in the first binding mode (i.e., the amino group at C4 of PP2) or with the carbonyl of Met341 in the second binding mode (i.e., the amino group at position 2 of the thiazole ring of **1**).
- (20) Catalyst software is distributed by Accelrys, Inc., San Diego, CA.
- (21) Further information can be found at the web site: <http://www.asinex.com/prod/gold.html>.
- (22) GRID 21; Molecular Discovery Ltd, 215 Marsh Road, Pinner, Middlesex, UK.
- (23) Details on the software can be found at the Molecular Discovery web page http://www.moldiscovery.com/soft_volsurf.php.
- (24) MacroModel, version 8.5. Schrodinger, L.L.C., 2003.
- (25) Nagar, B.; Hantschel, O.; Young, M. A.; Scheffzek, K.; Veach, D.; Bornmann, W.; Clarkson, B.; Superti-Furga, G.; Kuriyan, J. Structural basis for the autoinhibition of c-Abl tyrosine kinase. *Cell* **2003**, *112*, 737–740.
- (26) Hetenyi, C.; van der Spoel, D. Efficient docking of peptides to proteins without prior knowledge of the binding site. *Protein Sci.* **2002**, *11*, 1729–1737.
- (27) Ren, J.; Esnouf, R.; Garman, E.; Somers, D.; Ross, C.; Kirby, I.; Keeling, J.; Darby, G.; Jones, Y.; Stuart, D. High-resolution structures of HIV-1 RT from four RT-inhibitor complexes. *Nat. Struct. Biol.* **1995**, *2*, 293–302.
- (28) Ragno, R.; Mai, A.; Massa, S.; Cerbara, I.; Valente, S.; Bottoni, P.; Scatena, R.; Jesacher, F.; Loidl, P.; Brosch, G. 3-(4-Aroyl-1-methyl-1H-pyrrol-2-yl)-N-hydroxy-2-propenamides as a New Class of Synthetic Histone Deacetylase Inhibitors. 3. Discovery of Novel Lead Compounds through Structure-Based Drug Design and Docking Studies. *J. Med. Chem.* **2004**, *47*, 1351–1359.
- (29) Cona, A.; Manetti, F.; Leone, R.; Corelli, F.; Tavladoraki, P.; Polticelli, F.; Botta, M. Molecular Basis for the Binding of Competitive Inhibitors of Maize Polyamine Oxidase. *Biochemistry* **2004**, *43*, 3426–3435.
- (30) Further information can be found at the web site: <http://www.accelrys.com/products/catalyst/catalystproducts/jubilant.html>.

JM060236Z